Sensitivity analysis study on the effect of the fluid mechanics assumptions for the computation of electrical conductivity of flowing human blood

Gian Marco Melito [a],*, Thomas Stephan Müller [b], Vahid Badeli [c], Katrin Ellermann [a], Günter Brenn [b], Alice Reinbacher-Köstinger [c]

[a] *Institute of Mechanics, Graz University of Technology, Kopernikusgasse 24/IV, 8010 Graz, Austria*
[b] *Institute of Fluid Mechanics and Heat Transfer, Graz University of Technology, Inffeldgasse 25/F, 8010 Graz, Austria*
[c] *Institute of Fundamentals and Theory in Electrical Engineering, Graz University of Technology, Inffeldgasse 18/I, 8010 Graz, Austria*

ARTICLE INFO

ABSTRACT

Impedance cardiography is a non-invasive methodology for measuring cardiodynamic parameters, such as stroke volume and heart rate, as well as cardiac output. For the measurement, the electric conductivity of blood is important. The conductivity of blood depends on various parameters, such as the haematocrit value as well as the red blood cells' (RBC) shape and orientation. In models, the response is usually affected by uncertainty, which may lead to inaccurate medical diagnosis. Therefore, a ranking of the influence of the model's input factors may be necessary. Also, physically and physiologically correct assumptions are fundamental for the accuracy of the model. The basis for predicting the conductivity of blood in this study is the Maxwell–Fricke theory, which allows computing the electrical bulk conductivity of quiescent blood. For flowing blood, fluid mechanics has to be coupled in the modelling phase.

Nevertheless, some assumptions may lead to invalid or inaccurate results. Based on a global sensitivity analysis, this work shows which fluid mechanical assumptions are incorrect and should be avoided. Moreover, positive effects based on accurate rheological modelling of the fluid properties are shown, and the factors with a decisive influence on the computed conductivity change of flowing blood are illustrated.

1. Introduction

Blood is a heterogeneous suspension of several components, consisting of plasma as the carrier fluid, as well as erythrocytes (red blood cells), leukocytes (white blood cells) and thrombocytes (platelets) as the cellular content. The fluid is physically complex and, due to its physiological importance, its chemical and physical properties have been studied in numerous scientific fields, [1–8].

It is generally assumed that the physical properties of whole blood, such as the viscosity, i.e. its resistance to rates of deformation, and the electrical conductivity, are mainly determined by the properties of the red blood cells (RBCs) and the surrounding blood plasma. Furthermore, the electrical conductivity of blood is a crucial factor for electrical bioimpedance measurement applications in clinical settings [9–11].

The electrical properties of stationary blood depend mainly on the volume fraction of RBCs in the blood plasma, namely the haematocrit [12], RBCs' shape and orientation, and the temperature of the blood. In [13], the research on electrical conductivity began from a dilute suspension of spherical and ellipsoidal isolating particles in an electrolyte. From there, the findings produced the Maxwell–Fricke theory, which allows accurate calculation of the conductivity of stationary blood with randomly oriented RBCs as a function of haematocrit. To study electrical properties on flowing blood, [14] elaborated the theory quantitatively by introducing a Couette and successively a Poiseuille flow, and adding probability distributions for the orientation angles of RBCs. Within the Couette flow, the distribution of RBCs' orientation angles are dependent on the flow's shear rate until an orientation equilibrium is reached; the equilibrium of orientation distribution appears at low shear stress for high haematocrit values. Furthermore, after equilibrium is reached, the viscosity decreases continuously due to deformation of the RBCs. The reduction of viscosity is also confirmed at the breakup of rouleaux at low shear rates, a phenomenon leading to viscosity change. Regarding the Poiseuille flow, it is concluded that the RBCs orientation is crucial for blood conductivity.

Years later, the Maxwell–Fricke theory was tested for human blood in Poiseuille flow [15]. It was concluded that the cell orientation is the dominant cause of the electrical conductivity changes of blood, although large deformations of the RBCs occur. However, [16] and [17]

---

* Corresponding author.
E-mail address: gmelito@tugraz.at (G.M. Melito).

showed that if only the orientation of RBCs is considered, the conductivity changes do not depend on the shear rate for higher haematocrit levels (above 20%). Therefore, since an equilibrium orientation of the RBCs is reached at a low shear rate, for higher shear rates the conductivity changes are due to deformation of RBCs.

In [18], the Maxwell–Fricke theory was used to explain the dependency of the electrical conductivity of blood on its flow condition in a cylindrical tube. For this setup, the authors assumed a shear-rate independent viscosity fluid in a steady flow, in which RBCs are oblate ellipsoids that get deformed and oriented, given the flow condition. Since the conductivity of RBCs is very low at frequencies below 3 MHz, the current distribution in the suspension and thus the mean conductivity of this domain changes with the altered RBCs condition and configuration. This study leaves the electrical conductivity change of blood through the aorta due to its pulsatile flow condition unexplored.

To overcome this issue, [19–21] introduced a study on the impact of pulsatile blood flow on the electrical conductivity of blood in a cylindrical tube with rigid walls, using the flow theory developed by [22]. In this case, it was visible, both theoretically and experimentally, that during the acceleration phase of the fluid, i.e. the systolic phase of the cardiac cycle, a robust linear relationship between the average velocity and the conductivity of blood exists. The computed impedance shows differences in both systole and diastole related to the same average velocity. The latter phenomenon introduced a significant new insight into the physiological origins of impedance variations in bioimpedance methods. Developments performed in [23] include an elastic tube instead of a rigid one for the domain of the model. It results in highlighting the strong influence of the centre-line velocity value and the low impact of the wall elasticity on the electrical conductivity of blood.

Blood exhibits non-Newtonian behaviour dominated by shear thinning, which must be accounted for in simulating blood flows of the human body. Many models for blood flow, including the sources mentioned above, however, are subject to basic assumptions which may differ from the physical reality. Examples relate to the state of flow and the fluid dynamic behaviour upon deformation. E.g. the flow is modelled either steady or pulsating.

The rheological behaviour of blood is highly complex because its exact composition is more or less unique for each person. Broken down to the most important influencing factor regarding viscosity, the haematocrit value varies from person to person in a certain range for average women and men (adult males: 42 %-54 %; adult women: 38 %-46 % [24]). However it may differ by 4 %-7 % due to pregnancy [25] or exceed 60 % for professional athletes [26].

The present work focuses on analysing the electrical conductivity of flowing blood through a variance-based global sensitivity analysis (gSA) [27] by considering different flow situations (steady or pulsating) and rheological behaviour (Newtonian or non-Newtonian). Variance-based gSA can be performed with Monte Carlo method, which requires a high number of model simulations [28]. However, when dealing with complex model structure, surrogate models are usually preferred. Herein, the Polynomial Chaos Expansion (PCE) is used as surrogate model for the assessment of the sensitivity indices [29].

The uncertainty in computational models can originate from two different sources: in the model's input parameters and in the model selection. To reduce the first, a well-known uncertainty and sensitivity analysis is performed based on the assessment of the sensitivity indices from the PCE, see [30]. As for the model selection analysis, a discrete variable, namely the *trigger*, is added in the input space of the surrogate model. To the knowledge of the authors, the latter approach is innovative and not found in the literature.

The uncertainty quantification of the model selection was introduced with a Bayesian approach [31], where the posterior probabilities of all competing models are computed. The method, named Bayesian Model Averaging (BMA) [32], highlights the need for considering the uncertainty in the model selection to avoid over-confident inference

and decision. A latest application of BMA can be found in [33] where the best model choice is compared with the computed posterior probability. Lately, the approach was illustrated in [34] for the scope of sensitivity analysis and then applied in [35]. Other applications of model selection are found in countries composite indicators [36–38], geological analysis of potential oil basins [39], and CO_2 storage ability [33]. However, they all use Monte Carlo method to assess the sensitivity of several competing models. Therefore, a trigger variable in the input space of the surrogate model is introduced in this paper.

In the current study, different flow properties are studied by the trigger variable that simulates the change in the model assumption, i.e. emulating a switch behaviour. Differences between steady and pulsating flow with different fluid types (Newtonian or non-Newtonian) are predicted. The input space will also include different properties of the blood, distinguishing different patient-specific cases. In the pulsating case, the gSA will focus on the computation of the conductivity of blood in one cardiac cycle as a model output. The study aims to provide a more profound understanding of the mechanisms governing the value of the conductivity of flowing blood. The differences in the conductivity of blood due to the varied model parameters will lead to conclusions on the model sensitivity for this study case.

The paper is structured as follows: in Section 2 both the conductivity and the fluid models are illustrated. The first refers to the implementation of the state-of-the-art model for the computation of the conductivity of flowing blood. In the second, the pulsating flow condition and its particular case, i.e. steady flow, are referred to both the Newtonian fluid and the non-Newtonian one. Also, a non-dimensional formulation is derived in order to reduce the complexity of the model with respect to parameter variation and physiological ranges of the parameters. Successively, in Section 3, the gSA technique that is used in this study is explained, with particular attention to the variance-based approach and the use of the surrogate modelling of the polynomial chaos expansion. Results are shown and discussed in Section 4. In Section 5, the conclusions of the study are illustrated.

2. Models

The electrical conductivity of the blood is computed by assuming the fluid to be a dilute suspension of ellipsoidal particles [12,13]. The fluid is flowing in a straight and rigid pipe, where the RBCs, surrounded by plasma, are considered to be at the centre of each control volume [18]. The control volumes are given by the fluid domain discretization. The RBCs are oriented and deformed due to the shear stress induced by the fluid.

2.1. Electrical characterization of blood

The conductivity of flowing blood was initially modelled by [18] for a Newtonian fluid in steady laminar flow through a rigid tube of cylindrical shape. This model extends the Maxwell–Fricke theory by introducing orientation and deformation terms of RBCs in the flow. Here, different shear stress thresholds exert different orientation conditions of the RBCs. In [21], the model was extended by incorporating a pulsatile flow and different orientation effects. Thus, the assumption taken in [21] for the computation of electrical conductivity of blood are herein considered and applied.

2.1.1. Orientation and deformation of RBCs

RBCs are subject to orientation and deformation in flowing blood due to shear rate. Only two states of orientation for the RBCs are considered, namely: a random orientation as in flipping disc behaviour, and a stable orientation as in liquid drop behaviour. In the latter, given that the RBCs are aligned with their major $2b_0$ axis, see Fig. 1, within ±20° from the axial and dominant flow direction, RBCs are assumed to be parallel to the direction of flow [40].
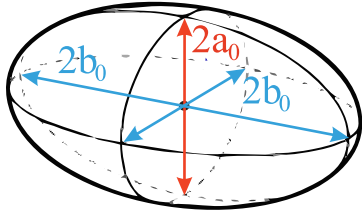
Fig. 1. Red blood cell modelled as an ellipsoidal particle.

Fig. 2. Geometry of the flow domain (not to scale).

When a pulsation of the flow is present, the time delay in the alignment of the RBCs to the flow field has to be accounted for. Such effect highly depends on the shear rate experienced by the cells and by the acceleration of the flow [4,41]. To tackle the orientation rate as a function of the shear rate, the function $f(r)$ at a distance r from the pipe axis, as introduced by [40], is shown as:

$$f(r) = \frac{n}{n_0} = \frac{\tau_o^{-1}(r)}{\tau_d^{-1}(r) + \tau_o^{-1}(r)}, \tag{1}$$

where n_0 is the total number of RBCs per unit volume, of which n are parallel to the flow, τ_o is the time constant for parallel orientation of cells, and τ_d is the time constant for the aligned cells to disorient in randomly oriented cells. The formulations of τ_o and τ_d are expressed in [40] as proportional to the inverse of the shear rate for τ_o, and as proportional to the inverse of the square root of the shear rate for τ_d.

Consider the RBCs as ellipsoidal particles with one symmetry axis of length $2a_0$ and two axes of equal length $2b_0$, s.t. $a_0 < b_0$, see Fig. 1. An erythrocyte with initial axes ratio a_0/b_0 is deformed into $a_d(r)/b_d(r)$ due to shear stress present in a pipe flow. This deformation is inversely proportional to the membrane shear modulus μ of the cells [18] and it is described as:

$$\frac{a_d(r)}{b_d(r)} = \frac{a_0}{b_0} \left[1 + \frac{\hat{\tau}(r) b_0}{4\mu} \right]^{-3}. \tag{2}$$

The magnitude of the shear stress tensor $\boldsymbol{\tau}$ is calculated by

$$\hat{\tau}(r) = \sqrt{\boldsymbol{\tau} : \boldsymbol{\tau}}. \tag{3}$$

This quantity depends on the position in the flow field and relates the state of deformation of the RBCs to the state of flow.

2.1.2. Conductivity of blood

The conductivity of blood is then computed from the Maxwell–Fricke theory, with the formulation introduced by [18], in which the conductivity of blood of a control volume $\sigma_{cv}(r)$ is given by:

$$\frac{\sigma_{cv}(r)}{\sigma_{pl}} = \frac{1 - H}{1 + (C(r) - 1)H}, \tag{4}$$

where σ_{pl} is the conductivity of the blood plasma in $S \cdot m^{-1}$, H is the haematocrit level of the blood, and $C(r)$ is the term accounting for the orientation and the deformation of RBCs at a radial location r in the pipe. In particular, the RBCs are considered impermeable to the electrical field for frequencies in the range of several hundred kHz, and therefore their amount in the blood volume is particularly significant. The following formulation gives the calculation of $C(r)$ [21]:

$$C(r) = f(r)C_b + (1 - f(r))C_r, \tag{5}$$

where $f(r)$ is the function for the orientation of RBCs from (1), and C_b and C_r are terms that account for the alignment of RBCs. C_r is the average of the C values for each axis alignment to the flow as in:

$$C_r = \frac{1}{3}(C_a + 2C_b), \tag{6}$$

where $C_a = 1/M$, $C_b = 2/(2 - M)$, and M is the deformation term computed as

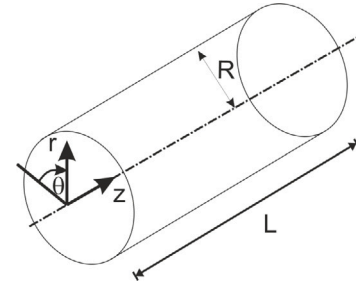$$M(a < b) = \frac{\phi - \frac{1}{2}\sin(2\phi)}{\sin^3 \phi} \cdot \cos\phi; \tag{7}$$

$$\cos\phi = \frac{a_d(r)}{b_d(r)}. \tag{8}$$

By substituting Eq. (2) in Eq. (8), the two models are coupled, i.e. the electrical conductivity model and the fluid dynamics model. The bulk conductivity of blood is computed as the integral of the control volume's conductivity over the cross-sectional area of the pipe of radius R as:

$$\sigma_{bl} = \frac{2}{R^2} \int_0^R \sigma_{cv}(r) r \, dr. \tag{9}$$

Finally, given the conductivity of stationary blood σ_{st} in which orientation and deformation of RBCs do not take place [15], the conductivity change of blood against its stationary value, expressed in percent, is computed as:

$$\Delta\sigma_{bl} = \left(\frac{\sigma_{bl} - \sigma_{st}}{\sigma_{st}} \right) \cdot 100. \tag{10}$$

2.2. Dynamics of blood flow

For the present study, the flow of blood through a cylindrical vessel with circular cross section is simulated, comparing steady and unsteady flow of blood modelled as a Newtonian or a non-Newtonian liquid. The study is based on an analytical description of the Newtonian, and on numerical simulations of the non-Newtonian flows.

The flow domain is a section of a straight pipe with a circular cross section of constant diameter $D = 2R = 25 \times 10^{-3}$ m. The section is 100 D long. The symmetry axis of the pipe is the z axis of a cylindrical coordinate system, as sketched in Fig. 2. The domain and the flow field are axisymmetric around the z axis, i.e., there is no dependency on the polar angular coordinate θ. Numerically, the flow is nonetheless treated as three-dimensional.

2.2.1. Governing equations

The fluid flowing through the pipe is assumed to be incompressible, i.e., its density ρ is treated as constant. For this case, the mass balance reduces to the requirement that the velocity field must be solenoidal, i.e.,

$$\nabla \cdot \boldsymbol{u} = 0. \tag{11}$$

Neglecting body forces, the vectorial momentum balance reads

$$\rho \left[\frac{\partial \boldsymbol{u}}{\partial t} + (\boldsymbol{u} \cdot \nabla)\boldsymbol{u} \right] = -\nabla p + \nabla \cdot \boldsymbol{\tau}, \tag{12}$$

where $\boldsymbol{\tau}$ is the extra stress tensor and p the pressure.

The rheological constitutive equation relates the extra stress to the velocity field. In the present study, two types of rheological behaviour of the liquid are considered: a non-Newtonian inelastic and shear-thinning, on the one hand, and the Newtonian one on the other.
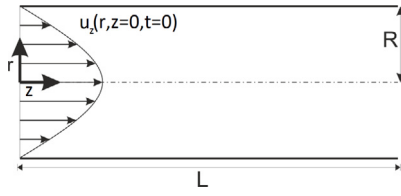
Fig. 3. Flow domain with inlet velocity profile at time $t = 0$ (not to scale).

Non-Newtonian inelastic shear-thinning - the generalized Newtonian model. As the rheological constitutive equation for the non-Newtonian liquid we select the Generalized Newtonian model given by [42] as

$$\boldsymbol{\tau} = 2\eta(\dot{\gamma})\boldsymbol{D}; \quad \dot{\gamma} = \left(2\mathrm{tr}\boldsymbol{D}^2\right)^{1/2} \tag{13}$$

where the shear rate $\dot{\gamma}$ is determined from the second invariant of the rate-of-deformation tensor [43] $\boldsymbol{D} = \left(\nabla\boldsymbol{u} + (\nabla\boldsymbol{u})^{\mathsf{T}}\right)/2$, with the velocity gradient $\nabla\boldsymbol{u}$.

The dynamic viscosity $\eta(\dot{\gamma})$ as a function of the shear rate is represented by the Carreau model [44]

$$\eta(\dot{\gamma}) = \eta_{\infty} + (\eta_0 - \eta_{\infty})\left[1 + (\lambda\dot{\gamma})^2\right]^{(n-1)/2}, \tag{14}$$

which is known to well represent shear-thinning liquid behaviour. In the model, η_0 represents the zero-shear viscosity (1st Newtonian plateau) and η_{∞} the limiting value of the viscosity for high shear rates (2nd Newtonian plateau). λ and n are parameters determining the shape of the function $\eta(\dot{\gamma})$. In the specification of this function for the computational analysis, the four parameters are determined by fitting (14) to experimental data from blood rheometry.

Special case of shear rate-independent viscosity - the Newtonian model. A Newtonian fluid has a shear rate-independent dynamic viscosity. Therefore its rheological constitutive equation reduces from (13) to

$$\boldsymbol{\tau} = 2\eta_{\mathrm{bl}}\boldsymbol{D}, \tag{15}$$

where η_{bl} is the dynamic viscosity of the blood treated as Newtonian. A model well-established in the literature for determining the viscosity of blood as a function of the haematocrit for a Newtonian rheological model is due to [1]. The determining equation reads

$$\eta_{\mathrm{bl}} = \eta_{\mathrm{pl}}\left[1 + 2.5H + 7.35H^2\right], \tag{16}$$

where η_{bl} and η_{pl} are the dynamic viscosity of blood and plasma, respectively, and H is the haematocrit represented as the volume fraction of red blood cells.

2.2.2. Initial and boundary conditions

Pulsating flow. In the numerical simulations, the flow is determined by a prescribed time-dependent volumetric flow rate and the corresponding velocity profile at the inlet of the pipe in Fig. 3. This profile is set parabolic at the inlet and evolves hydraulically in the flow direction z. The pipe section is long enough to ensure fully developed state at the outlet $z = L$. The flow rate of the pulsating flow is composed of a steady component Q_{mean} and a time-dependent component $Q_{\mathrm{osc}}(t)$. For the present study, the time dependence is set to be sinusoidal, i.e.,

$$Q(t) = Q_{\mathrm{mean}} + Q_{\mathrm{osc}}(t) = Q_{\mathrm{mean}} + \hat{Q}_{\mathrm{osc}} \cdot sin(\omega t), \tag{17}$$

where $\omega = 2\pi f$ is the angular frequency of the pulsation with frequency f, and $\hat{Q}_{\mathrm{osc}}$ is the pulsation amplitude. The volumetric flow rate equivalent velocity is given as $\bar{u}$, and $\hat{u}_{\mathrm{osc}}$ is the volumetric flow rate equivalent pulsation amplitude given as

$$u(t) = \frac{Q(t)}{A} = \bar{u} + u_{\mathrm{osc}}(t) = \bar{u} + \hat{u}_{\mathrm{osc}} \cdot sin(\omega t). \tag{18}$$

The corresponding heart rate is computed in beats per minute (bpm) by converting the frequency f from s^{-1} to min^{-1}. The boundary conditions for the velocity components u_z, u_r, u_θ at the inlet are imposed in the following forms:

$$u_z(r, z = 0, t) = \frac{2Q(t)}{A}\left(1 - \frac{r^2}{R^2}\right) \quad r \in [0, R]; \tag{19}$$

$$u_r(r, z = 0, t) = u_\theta(r, z = 0, t) = 0 \quad r \in [0, R]. \tag{20}$$

The boundary conditions at the pipe wall represent the no-slip condition

$$u_z(r = R, z, t) = u_r(r = R, z, t) = u_\theta(r = R, z, t) = 0 \quad \forall z, t, \tag{21}$$

Steady flow. The steady flow is the special case where all the properties of the flow are time-independent. The boundary conditions for the velocity components at the pipe inlet read

$$u_z(r, z = 0) = \frac{2Q_{\mathrm{mean}}}{A}\left(1 - \frac{r^2}{R^2}\right) \quad r \in [0, R]; \tag{22}$$

$$u_r(r, z = 0) = u_\theta(r, z = 0) = 0 \quad r \in [0, R]. \tag{23}$$

The steady-state no-slip conditions at the pipe wall are analogous to Eq. (21).

For both the unsteady and the steady simulations, the pressure at the outlet $z = L$ was set to zero. The inlet pressure was obtained as a part of the solution of the flow problem.

2.3. Non-dimensional parameters

The mechanical behaviour of flowing fluids is governed by sets of non-dimensional parameters. The parameters are defined as groups of quantities characterizing the flow and the fluid, such as characteristic velocities, length scales and fluid material properties. For the present physiological context, the values of such parameters are known from the literature. We mention the flow velocity, pulsation (heart beat) frequency, vessel diameter and blood viscosity. From these values, the values of the non-dimensional parameters are characterized in the uncertainty analysis of this article.

With account for the unsteady case, the present flow is governed by the six parameters $\bar{u}$, $\hat{u}_{osc}$, ω, D, ρ and η. Given the three dimensions kg, m and s involved, these parameters form the three non-dimensional groups

$$\mathrm{Re} = \frac{\rho\bar{u}D}{\eta}; \quad \mathrm{Wo} = D\sqrt{\frac{\omega\rho}{\eta}}; \quad \text{and} \quad \varphi = \frac{\hat{u}_{osc}}{\bar{u}}, \tag{24}$$

where φ may be interpreted as the ratio of the corresponding flow rates, $\hat{Q}_{osc}/Q_{\mathrm{mean}}$, also.

The first non-dimensional group is the Reynolds number Re. It represents the ratio of convective to diffusive transport of momentum, with the volumetric flow rate equivalent velocity $\bar{u}$, the diameter D of the pipe, and the density and dynamic viscosity of the fluid, ρ and η, respectively. Defining the Reynolds number for fluids with variable viscosity requires a special treatment. The form of the generalized Reynolds number in non-Newtonian flow proposed by [45] for a power law fluid was re-derived for the present Carreau fluid to yield

$$\mathrm{Re}_{\mathrm{gen}} = \frac{\bar{u}^2\rho}{\frac{3m+1}{4m}\left(\frac{\bar{u}}{D}\right)} \cdot \left[\eta_{\infty} + (\eta_0 - \eta_{\infty})\left[1 + \left(\lambda\frac{3m+1}{4m}\left(8\frac{\bar{u}}{D}\right)\right)^2\right]^{\frac{n-1}{2}}\right]^{-1}. \tag{25}$$

The coefficient m, which represents a logarithmic derivative of the pressure gradient with respect to a representative shear rate, is calculated as

$$m = \frac{\eta_{\infty} + (\eta_0 - \eta_{\infty})\left[\left[1 + (\lambda\dot{\gamma}_w)^2\right]^{(n-1)/2} + (\lambda\dot{\gamma}_w)^2(n-1)\left(1 + (\lambda\dot{\gamma}_w)^2\right)^{(n-3)/2}\right]}{\eta_{\infty} + (\eta_0 - \eta_{\infty})\left[1 + (\lambda\dot{\gamma}_w)^2\right]^{(n-1)/2}}, \tag{26}$$

with the wall shear rate $\dot{\gamma}_{\text{wall}} = \frac{3m+1}{4m}\left(8\frac{\bar{u}}{D}\right)$. For each value of the generalized Reynolds number, m was iteratively calculated, starting from an initial value, calculating the wall shear rate from this value, and using this wall shear rate to calculate a new m, and so forth. This process was repeated until the difference between two successive values of m was below 10^{-5}.

The second non-dimensional group in (24) is the Womersley number, which represents the ratio of the time scale for diffusive momentum transport to the pulsation period. In the case of the non-Newtonian fluid model, the dynamic viscosity varies in the flow field. Therefore, for calculating the Womersley number, the kinematic viscosity is expressed using the generalized Reynolds number to make it read

$$\text{Wo} = \sqrt{\frac{D\omega}{\bar{u}}\text{Re}_{\text{gen}}}. \tag{27}$$

The pulsating nature of the flow is represented by the non-dimensional group φ in (24). Using this group, (17) transforms into

$$Q(t) = Q_{\text{mean}} \cdot [1 + \varphi \cdot sin(\omega t)] \tag{28}$$

Different magnitudes of φ determine the flow as follows:

$$\varphi = \frac{\hat{u}_{\text{osc}}}{\bar{u}} \begin{cases} \ll 1 \text{ - steady flow rate dominating} \\ \gg 1 \text{ - oscillating flow rate dominating} \end{cases} \tag{29}$$

2.4. Numerical solutions

For non-linear material behaviour, the analysis of the flow field requires a numerical method. The model Eqs. (11) and (12) were solved with the finite-volume method of the open-source software *OpenFOAM*. Due to the axial symmetry, the flow field in the pipe was reduced to a wedge of 5° in the polar angular direction, setting symmetry boundary conditions at the angular faces. The wedge was discretized into 1500 hexahedral and prism cells, with a refined grading towards the pipe wall in order to resolve correctly the gradients on the wall surface. A mesh convergence study was performed with Newtonian fluid properties, and the velocity profile at the outlet from the pipe section was compared to match the analytical solution of the laminar Hagen–Poiseuille flow. With the above number of cells, a further refinement of the discretization did not change the results appreciably. For the numerical solution, a second-order implicit scheme was chosen for time. Gradient and divergence schemes were calculated with second-order central differences. The non-orthogonality of wall-normal gradients was taken into account by using an appropriate correction scheme. For evaluating the results it was ensured that the flow at the outlet from the pipe section, $z = L$, was developed. Additionally, for the unsteady simulations, a periodic solution was obtained. Due to the maximum values of the Reynolds number studied, the computations involved laminar flow.

2.5. Analytical solution

In the case of the Newtonian material behaviour, which is linear, and given the symmetry of the flow domain, the hydraulically developed flow may be calculated analytically, even in the unsteady case. The result is that the radial and the polar angular velocity components are zero throughout the flow field. The analytical solution for the z-velocity component is represented non-dimensionally as [46]

$$u_z^*(r^*,t^*) = 2\left(1 - r^{*2}\right) + \Re\left\{e^{i2\pi t^*}\frac{32i\hat{p}^*}{\text{Wo}^2}\left[1 - \frac{J_0\left(r^*\sqrt{-i}\text{Wo}/2\right)}{J_0\left(\sqrt{-i}\text{Wo}/2\right)}\right]\right\}. \tag{30}$$

Here $\Re$ denotes the real part of the complex term in the braces, and i the imaginary unit. J_0 is a Bessel function of the first kind and of 0-th order. The quantities denoted by a star in (30), i.e. u_z^*, r^*, t^* and $\hat{p}^*$, are derived through nondimensionalization with respect to the following

reference quantities: $\bar{u}$ for the velocity, R for length and coordinates, the period of the pulsation $T = 2\pi/\omega$ for the time, and $\rho\bar{u}^2$ for the pressure. The analytical solution is based on a time-dependent pressure gradient driving the flow. $\hat{p}^*$ is the non-dimensional amplitude of the time-dependent pressure gradient. In the present analysis, a volumetric flow rate equivalent to that pressure gradient was applied.

3. Method

Uncertainty and sensitivity analysis are fundamental steps in model building and they represent an important role in the decision making process that results from model simulations [47]. Sensitivity analysis is used to extract the information, rooted into computational models, about how much the uncertainty in the input factors affects the model output(s). Several methods are used to rank the most influential variables on a quantity of interest and to assess their level of interactions [48,49].

Sensitivity analysis is classified as local when it focuses on the impact of one input random variable in its vicinity for a small perturbation. In other words, one input parameter at a time is varied while the others are kept fixed [50]. Examples of some local sensitivity analysis are finite difference computation [47], differential importance measure [51], elasticity measure [52], screening methods [47,53].

Alternatively, when multiple parameters are varied simultaneously and the analysis is performed over the whole input space, the sensitivity analysis is said to be global. Global sensitivity analysis (gSA) quantifies the uncertainty of the model quantity of interest (QoI) by looking at the uncertainty in all input parameters and their combination. gSA is also a powerful tool when it is used in calibrating the model to reproduce a physical process and it is based on the assumption that an information about the model inputs' probability distribution, joint or marginal, is provided [39].

Different methods have been developed for gSA [47]. Non-parametric methods are successful in case of model linearity and apply a regression of the model response to its input factors to produce measures as standard regression coefficient or the Pearson correlation coefficient. The variance-based methods base their analysis on the expected reduction in model output variance given the certainty of the model input factors. This method is built upon the ANOVA output variance decomposition, which is unique in case of independent input random variables [54–56]. From the variance decomposition, sensitivity measures such as Sobol indices can be developed [57]. Some other global sensitivity analysis methods are density-based method and transformation invariant method. The first considers the entire probability distribution of the quantity of interest, thus it does not focus the analysis on one particular distribution moment [58,59]. The second aims at transforming the output space when this is sparse or its range covers many order of magnitude [60,61].

A variance-based approach is used for the current study. In this case, the variance of the output is decomposed into a sum of contributions of the input space [29]. Since knowledge regarding the model is limited, in the sense that it is unknown whether its behaviour can be linear, additive, monotonic, or none of them, the choice of a variance-based approach is suitable. A model is defined to be additive when it is possible to differentiate the effects of each input parameter on the model's output [35] separately.

For the estimation of the Sobol indices as quantitative measures for the gSA, a surrogate model construction is employed, namely the polynomial chaos expansion. Alternatively, the use of Monte Carlo sampling or quasi-Monte Carlo sequences are adopted, but the cost of this computation is still affected by the high number of model calls [48].

3.1. Variance-based approach

One of the most used techniques in gSA is the variance-based method. Here, the output variance is apportioned in the sum of the contributions of each random variable. The mechanics of the variance-based method are initiated with the Sobol' decomposition of the model [57]. Consider a mathematical model as a function of an input random vector $\boldsymbol{x}$ of dimension M defined in the unit cube K^M, such as $Y = f(\boldsymbol{x})$. The Sobol' decomposition of the model reads

$$Y = f(x_1, \ldots, x_M) = f_0 + \sum_{i=1}^{M} f_i(x_i) + \sum_{1 \leq i < j \leq M} f_{ij}(x_i, x_j) + \cdots$$
$$+ f_{1,\ldots,M}(x_1, \ldots, x_M), \tag{31}$$

where f_0 is a constant and represents the average value of the model response. The uniqueness of the decomposition is granted by the orthogonality of the summands in (31) over the M-dimensional unit cube of the input space K^M. Each term of (31), is expressed as constant (32), univariate–(33), bivariate–(34), and multivariate-terms.

$$f_0 = \mathbb{E}[Y] \tag{32}$$

$$f_i = \mathbb{E}[Y|x_i] - -\mathbb{E}[Y] \tag{33}$$

$$f_{ij} = \mathbb{E}[Y|x_i, x_j] - -f_i - f_j - \mathbb{E}[Y]. \tag{34}$$

Considering the model input is defined as a random variable; its response will be random, its variance can also be decomposed with (31). By doing so, the first-order sensitivity index [62,63] (or first-Sobol' index) can be derived by the ratio of the partial variance due to the ith random variable and the total variance of the model. By definition, the first-Sobol' index is also a function of the conditional variance $\mathbb{V}(\mathbb{E}[Y|x_i])$ of the model output as:

$$S_i = \frac{\mathbb{V}[\mathbb{E}[Y|x_i]]}{\mathbb{V}[Y]}, \tag{35}$$

which represents the contribution of the random variable x_i to the change of the model output, without considering the effect of its interaction with other input variables. Therefore, a random variable x_i is considered to be influential (non-influential) to the model output if the conditional variance $\mathbb{V}(\mathbb{E}[Y|x_i])$ is large (small) enough to the variance of the quantity of interest. The first-order index identifies the level of influence of the single parameter on the output in the analysis. It does not give any information regarding the interaction of the parameter with other variables of the input space. It allows the use of the *Factor Prioritization* setting, that is the identification of the input factors that contain the most influence on the QoI, i.e. which one is the most responsible for the production of the model variation.

As expected, in (35), the bivariate- and multivariate-terms expressed in (33) and in (34) are missing. Thus, the need for a quantitative measure to account for the interaction effect among the input parameter has to be fulfilled. The total-order sensitivity index (or total-Sobol' index), which evaluates the total effect of such input parameter, has to account for the conditional variance of the output. The conditional probability is then computed over the whole input space except the ith random variable. This is described as $\boldsymbol{x}_{\sim i}$ and leads to the evaluation of the total-Sobol' index as:

$$S_i^T = 1 - \frac{\mathbb{V}[\mathbb{E}[Y|\boldsymbol{x}_{\sim i}]]}{\mathbb{V}[Y]} = \frac{\mathbb{E}[\mathbb{V}[Y|\boldsymbol{x}_{\sim i}]]}{\mathbb{V}[Y]}. \tag{36}$$

The total-order sensitivity index shows the degree of the influence of the input random variable alone on the QoI together with the interactions with other input factors. The total-order index is used to produce the *Factor Fixing* setting. Here, the lower values of the total-order index are analysed to decide which variable has no effect or low effect on the output, considering also its collaborations. As a consequence, they can be considered as model constants, and the model output will not be affected by such change. Together with the first- and total-order sensitivity indices, it is possible to compute the interaction terms of several degrees of interaction. However, the first and total indices together express the influence relationship of the input domain on the QoI sufficiently and avoid the need of computing high-order sensitivity indices, which may be computationally expensive [39].

3.2. Polynomial Chaos Expansion

The estimation of the Sobol indices, (35) and (36), can be performed with several numerical methods. A common one involves the use of Monte Carlo method. Here, a deterministic model is evaluated for a large sample collected from the input space of the model, and finally the conditional expectations in [71,72] are computed. However, this method requires a large number of samples, which might result impractical in some applications. An alternative solution is the construction of surrogate models, such as Polynomial Chaos Expansion (PCE), which allows to derive an analytical expression for the sensitivity indices [29, 30]. The PCE was introduced by [73] and implemented in the engineering world by [71]. It aims at representing random fields in a polynomial expansion based on orthogonal polynomials of probability measures [72].

A polynomial chaos expansion for a model of dimensionality M is formulated as:

$$Y(\boldsymbol{x}) \approx f_{\text{PCE}}(\boldsymbol{x}) = \sum_{\boldsymbol{\alpha} \in \mathcal{A}} y_{\alpha} \Psi_{\alpha}(\vec{X}), \tag{37}$$

where $\boldsymbol{\alpha} = (\alpha_1, \alpha_2, \ldots, \alpha_M)$ is a multi-index of a set $\mathcal{A}$ of $N_p = \binom{M+p}{p}$ for polynomials with a maximum degree p, the multivariate polynomials Ψ_{α} are defined as the product of univariate polynomials of degree α_i, i.e. ψ_{α_i} [28]. The univariate polynomials are generated following the Askey scheme for the composition of polynomials. As a final step, the estimation of the two sensitivity indices (35) and (36) is performed from the expansion coefficients y_{α} and evaluations of the analytical expressions of the normalization factor associated with the polynomial Ψ_{α} [74]. The expansion coefficients y_{α} can be estimated with projection or regression methods [29].

In this study, PCE is computed through the UQLab toolbox for Matlab [75].

### 3.3. Application to the model

The uncertainty sources in the present study are generated by both the physiological variability of the human body and the variation of data collected from model assumptions. Physiological parameters, such as aortic flow rate Q_{mean} and corresponding flow rate ratio φ, blood haematocrit H and density ρ, and heart rate f, present significant probability distribution variation [1,21,64–67]. Moreover, through literature research on the models that emulate the electrical conductivity of blood, it has been noticed that some of the input parameters vary substantially among different authors, i.e. the RBCs axes ratio a_0/b_0, the electrical conductivity of plasma σ_{pl} [15,21,68], and viscosity of plasma η_{pl} [21,67]. A uniform probability distribution function for all random variables is considered, due to the lack of prior information on their real probability distributions. Furthermore, this assumption allows to better emphasize the randomicity of different patient-specific cases. The ranges of the distributions, shown in Table 1, highlight the uncertainty that afflicts medical research. Their variation aims at producing different responses of the models and at analysing their influence through such models using a sensitivity analysis technique.

Different model assumptions are the basis of the sensitivity analysis to understand the importance of such hypotheses when computing the conductivity of blood. One of the questions that arose in the development of this study is: how complex should the fluid model be to give a reliable output of electrical conductivity change of flowing blood? Often models tend to simplify the fluid mechanics of the problem to avoid complexity and to reduce the computational effort. Therefore, it is the interest of this study to evaluate and quantify the importance of

Table 1
Input parameters of the model and their probability distribution properties used for sensitivity analysis.

Parameter	Notation	Probability distribution	Unit	Reference
Volumetric flow rate	Q_{mean}	$\mathcal{U}[3.20e{-}5, 1.82e{-}4]$	m^3/s	[64]
Flow rate ratio	φ	$\mathcal{U}[0.1, 1]$	–	[64]
Blood density	ρ	$\mathcal{U}[1050, 1060]$	kg/m^3	[21,65–67]
Haematocrit level	H	$\mathcal{U}[0.30, 0.70]$	–	[1]
RBCs axes ratio	a_0/b_0	$\mathcal{U}[0.11, 0.40]$	–	[15,21,68]
Conductivity of plasma	σ_{pl}	$\mathcal{U}[1.12, 1.57]$	S/m	[15,21,68]
Viscosity of plasma	η_{pl}	$\mathcal{U}[1.10e{-}3, 1.55e{-}3]$	Pa s	[1,21,67]
Heart rate	f	$\mathcal{U}[50, 100]$	min^{-1}	[69,70]
Trigger (model assumption)	trigger	[1, 2 or 3]	–	[15,18,20,21]
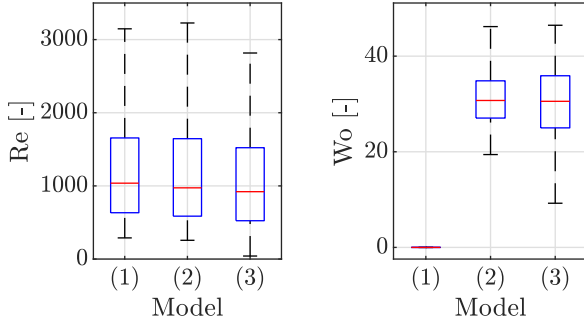
Fig. 4. Dimensionless Reynolds and Womersley number for the simulations of each model assumption.

Fig. 5. Leave-One-Out Error $\varepsilon_{\mathrm{LOO}}$ of the PCE for models (2) and (3). The computed error for the $\Delta\overline{\sigma}_{\mathrm{bl}}$ is indicated with the star marker (*), while for $\Delta\hat{\sigma}_{\mathrm{bl}}$ with the circle marker (o).

such choices concerning the evaluation of the conductivity of blood. The last random variable in Table 1, discretely distributed and referred to as the *trigger*, is used to analyse the differences in the output considering different model assumptions:

Model (1) Newtonian fluid and steady flow

Model (2) Newtonian fluid and pulsating flow

Model (3) Non-Newtonian fluid and pulsating flow

The experimental design is built so to explore the model's input space. The variability of the input space is also meant to simulate the randomicity of everybody's health condition and characteristics. It is therefore essential to analyse the functioning of different model assumptions in relation to the randomness of their corresponding input domain (Table 1). In order to assure the physiological ranges of the flow parameters with respect to the rheological parameters of the human body in modelling haemodynamics [76], the ranges of non-dimensional numbers characterizing the flow are calculated and depicted in Fig. 4, namely the Reynolds and the Womersley number. Given the fact that their distributions lead to laminar condition, the flow is considered laminar.

The conductivity change relative to stationary blood was determined to assess the QoI, as expressed in (10). In particular, given its variability over one cardiac cycle, its average value in time over the period is taken into account

$$\Delta\overline{\sigma}_{\mathrm{bl}} = \frac{1}{T}\int_0^T \Delta\sigma_{\mathrm{bl}}\,dt. \tag{38}$$

The reason for this choice is that such output holds more useful information about the behaviour of conductivity of blood over time. More importantly it is mostly used in the related scientific literature, instead of considering the conductivity of blood per se. The peak-to-peak amplitude of such signal over one cardiac cycle, referred as $\Delta\hat{\sigma}_{\mathrm{bl}}$, is also considered to be of interest to analyse the models' mechanics.

Two different sensitivity analyses have been performed. The first one is a sensitivity analysis *within* each model assumption, i.e. model (1), (2) or (3), to better understand their functioning and mechanics. This analysis is performed with a different sample size N_s of the input
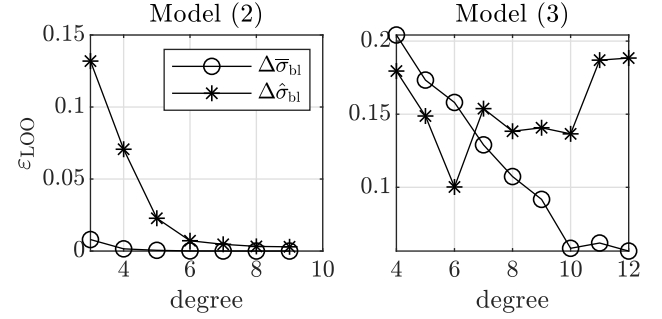
space, with the dimension $M = 8$, given that the trigger variable is considered constant for such computation. The high computational expenses of model assumption (3), i.e. non-Newtonian fluid and pulsating flow, constrains the number of performed simulations to $N_{s_3} = 500$. For trigger equal 1 or 2, the sample size is $N_{s_{1,2}} = 10000$ due to the availability of the analytical formulation for the fluid mechanics, which reduces the computational costs.

The second sensitivity analysis is then performed *among* the model assumptions and with the input space of dimension $M = 9$, since the last factor of Table 1 is assumed as a random variable. For this analysis, the number of simulations is $N_s = 1500$, so that each model assumption is run an equal amount of times.

The two sensitivity analyses, are computed from two different polynomial chaos expansions. The surrogate model for the analysis within each model assumption is resolved with ordinary least square method (OLS) [77,78] for the models (1) and (2), given the low computational costs. For model (3), due to the limited number of simulations, the least-angle regression (LARS) method [79] is selected. The degree of each expansion is selected at the minimum of the Leave-One-Out error $\varepsilon_{\mathrm{LOO}}$ [30,80] produced for different polynomial degrees. Therefore, as visible in Fig. 5, degree 7 is chosen for both QoIs in model (2). As for model (3), PCE is truncated at degree 10 for the cycle average $\Delta\overline{\sigma}_{\mathrm{bl}}$, and at degree 6 for the amplitude $\Delta\hat{\sigma}_{\mathrm{bl}}$. OLS method is selected for the sensitivity analysis among the model assumptions and the polynomial is truncated at degree 4, see Fig. 6. A PCE degree smaller than M suggests the exclusion in the PCE of some interaction terms. However, the employed basis-adaptive strategy detects and deletes negligible high-order interaction terms, reducing the dimensionality of the truncated polynomial expansion [79,81].

The *trigger* variable is included in the construction of the polynomial chaos expansion upon transformation into a uniformly distributed variable. Nonetheless, such transformation does not affect the accuracy of the surrogate model. By evaluation of the accurate PCE, a Monte Carlo method is chosen for the estimation of the Sobol indices among the model assumptions, (35) and (36).
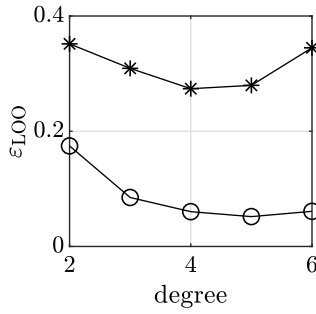
Fig. 6. Leave-One-Out error $\varepsilon_{\mathrm{LOO}}$ of the PCE for sensitivity analysis among the three model assumptions. The computed error for the $\Delta\overline{\sigma}_{\mathrm{bl}}$ is indicated with the star marker (*), while for $\Delta\hat{\sigma}_{\mathrm{bl}}$ with the circle marker (o).

4. Results and discussion

4.1. Uncertainty analysis

After performing the simulations for each model assumption, a first check on the reliability of the results was performed. In Fig. 7, the box plots of the cycle average of the conductivity change of blood $\Delta\overline{\sigma}_{\mathrm{bl}}$ (left) and its amplitude $\Delta\hat{\sigma}_{\mathrm{bl}}$ (right) are shown.

An overview of the distribution of the results of the QoIs is necessary to analyse the behaviour of different model assumptions and differences in their mechanics. Here, the distribution of the cycle average of the blood conductivity change of the model assumption (1) (Fig. 7 left, model (1)) shows inaccurate results. Its distribution is characterized by a median value slightly larger than zero and by a prolonged negative tail. As visible, such results are inaccurate in expressing the increment of conductivity of flowing blood. Theoretically, during the flow condition, RBCs are oriented and deformed by the shear rate. The steady flow assumption has been developed for the computation of the electrical conductivity of blood, given its simplicity and easiness in implementation. Results of its use are also compared to experimental results [18]; however, those comparisons stand only for a few particular cases and combinations of the input domain. Thus, since most of the distributions of the conductivity change $\Delta\sigma_{\mathrm{bl}}$ are below the zero value, model (1) indicates the inability of the steady flow assumption in computing such QoI, given the variability of the input parameters. Furthermore, due to the steadiness of the flow, the amplitude of the conductivity change of blood is absent, which stresses the inability of such assumption in emulating the nature of such measurement. As a consequence, the steady flow model assumption is not considered for the following sensitivity analysis.

The results for model assumptions (2) and (3) are not only comparable, but also more realistic when compared to the real behaviour of the $\Delta\sigma_{\mathrm{bl}}$ signal. In previous deterministic models [19–21], $\Delta\sigma_{\mathrm{bl}}$ is shown to oscillate between 10% and 20%. Lack of previous studies on the variation of such outputs for different fluid and flow assumptions lead to the conclusion that the present results are valid. The distributions of $\Delta\overline{\sigma}_{\mathrm{bl}}$ show good agreement both in the median value and the tail of the distributions. Regarding the distribution of the amplitude of conductivity change $\Delta\hat{\sigma}_{\mathrm{bl}}$, see the right plot in Fig. 7, the assumption of a non-Newtonian fluid highly increases the variability of this QoI. Such a phenomenon has to be further investigated through a sensitivity analysis among the models, with a particular interest in the output $\Delta\hat{\sigma}_{\mathrm{bl}}$. Nonetheless, both distributions show good agreement with the nature of the $\Delta\sigma_{\mathrm{bl}}$ signal, and are therefore considered as reliable results [19–21].

For the sake of completeness, the results of the pulsating flow models are shown in Fig. 8. Here, the average trends over the simulations of the conductivity change of blood, both for the Newtonian and non-Newtonian fluid in pulsating flow, are plotted over a normalized
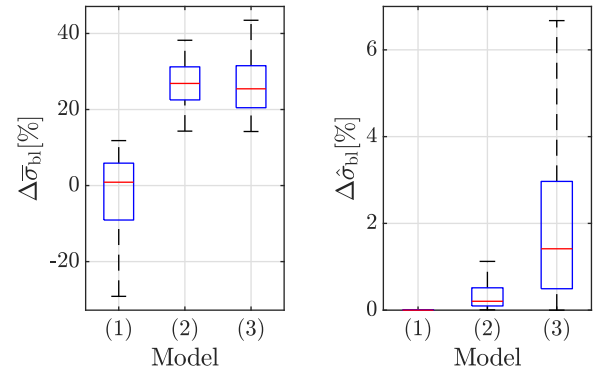

Fig. 7. Box plots of the cycle average of conductivity change of blood (left) and its peak-to-peak amplitude (right) for the three model assumptions.
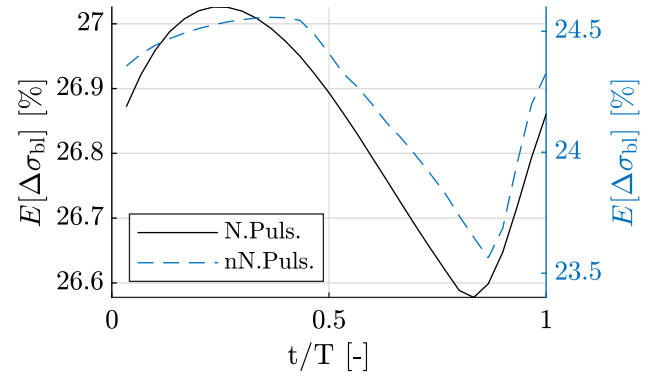

Fig. 8. Conductivity change of blood in time averaged over the simulations for a Newtonian (in black) and non-Newtonian fluid (in blue), both in a pulsating flow model assumption.

cardiac period. Noticeable is the similarity of expressing the delay in decelerating when compared to the input sinusoidal wave of the volumetric flow rate (Section 2.2.2), as researched in [21].

4.2. Sensitivity analysis

Before proceeding with the sensitivity analysis, an investigation of the behaviour of the model is performed with the use of a scatter plot, see Fig. 9, where the input parameters are projected in turn against the two QoIs. Here, the grey colour represents the use of the model (2) assumption, while the black one refers to model (3). Furthermore, the input space is normalized with respect to their input domain and $\Delta\hat{\sigma}_{\mathrm{bl}}$ is represented in log scale for better visualization.

The scatter plots show that $\Delta\overline{\sigma}_{\mathrm{bl}}$ is more sensitive to the variables haematocrit H and the RBCs axes ratio a_0/b_0, which display a strong linear relationship in both model assumptions. In addition, the volumetric flow rate Q_{mean} for model (2) also shows a linear trend, but all the other input factors do not exhibit particular influence. As for the amplitude of the conductivity change of blood $\Delta\hat{\sigma}_{\mathrm{bl}}$, a clear difference behaviour between the two model assumptions is visible. In model (2), variables such as haematocrit H, volumetric flow rate Q_{mean} and flow rate ratio φ demonstrate a higher influence on $\Delta\hat{\sigma}_{\mathrm{bl}}$. In model (3) however, while H seems to maintain its impact on this output, Q_{mean} influence decreases. Instead, the flow rate ratio φ shows a new strong linear trend. The output $\Delta\hat{\sigma}_{\mathrm{bl}}$ is also equally influenced by the RBCs axis ratio a_0/b_0 for both model assumptions.

Worthy of note is the difference in output domain coverage for $\Delta\hat{\sigma}_{\mathrm{bl}}$ when switching from model (2) to model (3), see Fig. 9 bottom row. For the latter, all the input variables show an exponential behaviour, apart from φ in case of Non-Newtonian fluid and pulsating flow assumptions,
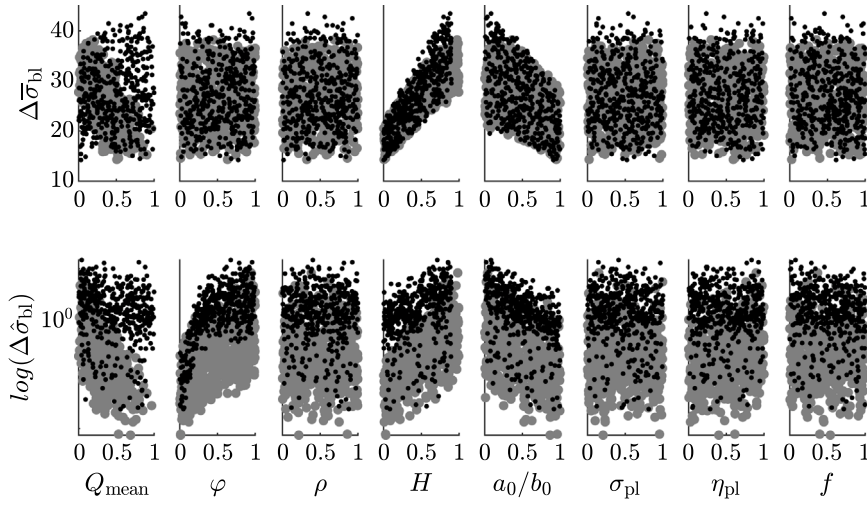
Fig. 9. Scatter plot of the two quantities of interest, cycle average of change of blood conductivity $\Delta\overline{\sigma}_{bl}$ and its amplitude $\Delta\hat{\sigma}_{bl}$, versus the model input parameters, normalized in their domain (Table 1). The third dimension, the colour, represents different model assumptions: grey for model (2) and black for model (3).
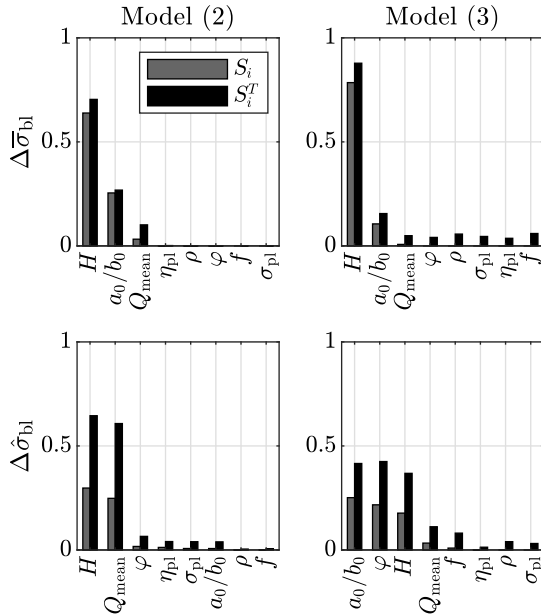

Fig. 10. Sensitivity indices on the mean value (top) and amplitude (bottom) of the conductivity change of blood for model 2 (Newtonian fluid and pulsating flow) and model 3 (non-Newtonian fluid and pulsating flow). The grey bars represent the first-order sensitivity index; the black bars the total order sensitivity index. The variables are sorted by first-order sensitivity index.

which suggest the presence of a level of interactions higher than for the output $\Delta\overline{\sigma}_{bl}$. The use of scatter plots aids in identifying influential parameters, however it can be deceiving and lead to refutation of influential parameters [34]. This motivates the use of a variance-based sensitivity analysis and the computation of Sobol' indices.

Sensitivity analysis results are plotted in Fig. 10. The top two figures refer to the first- and total-order Sobol' indices on the cycle average of the blood conductivity change $\Delta\overline{\sigma}_{bl}$ for models (2) and (3). In contrast, on the bottom, the indices refer to the amplitude of blood conductivity change $\Delta\hat{\sigma}_{bl}$.

Regarding the first-order sensitivity indices S_i of the output $\Delta\overline{\sigma}_{bl}$ (top figures in Fig. 10), the ranking of the most influential factors is similar for both model (2) and (3) having the haematocrit value of blood H as the most important one, followed by the RBCs axes

ratio a_0/b_0 and the volumetric flow rate Q_{mean}. The haematocrit value is the volume fraction of RBCs in the blood, thus proportional to the number of RBC, which are considered to be non-conductive for the electrical signal. The electrical signal follows the path with less resistance; indeed, it is eased by fewer RBCs or by many oriented and deformed cells. This result confirms the influence on the mean value in time of the $\Delta\sigma_{bl}$ of both the haematocrit value H and the RBCs axes ratio a_0/b_0 before the deformation of such cells takes place.

The interaction effect is estimated by the difference between the first- and total-order sensitivity indices. An analysis of the total order Sobol' indices S_i^T of the same output (black bars in the top two figures of Fig. 10), firstly highlights the presence of low interactions between the parameters; thus the model could be considered additive in the output $\Delta\overline{\sigma}_{bl}$. Secondly, it drives the discussion in considering variables as constant values for the model, i.e. applying the *Factor Fixing* setting, since any variation in their value will not affect the considered model's response. Such variables are the viscosity of plasma η_{pl}, the conductivity of plasma σ_{pl}, the flow rate ratio φ, the heart rate f and the blood density ρ.

Different behaviour is shown for the sensitivity analysis on the amplitude of blood conductivity change $\Delta\hat{\sigma}_{bl}$, see Fig. 10 bottom figures. Model (2) (left picture) confirms that the haematocrit value gives the principal influence on the output H mainly and secondly the volumetric flow rate Q_{mean}. Such influence is explained by the presence of H in both (16) for the computation of the viscosity of blood and in the Maxwell–Fricke theory (4). Both equations form the basis for calculating the blood conductivity and the fluid mechanical model, so affecting the shear rate of the flow and then the RBCs deformation. To be noticed is also the increment in interaction terms in the model for this particular output, contrary to what was discussed for $\Delta\overline{\sigma}_{bl}$, see Fig. 10 left-top.

By looking at the sensitivity analysis results for the non-Newtonian fluid model, Fig. 10 right-bottom, it is clear how the mechanics for the computation of the electrical conductivity is altered. Here, the highest first-order sensitivity indices are recorded in the flow rate ratio φ, and in the RBCs axes ratio a_0/b_0. Also, the haematocrit level H shows a high influence on the model's QoI, but its value is not the highest recorded. The reason for such change of mechanics has to be found in the change of formulation between the Newtonian and the non-Newtonian fluid models. In the non-Newtonian formulation, the viscosity model of [2] (16) is not implemented, given the non-linearity of the viscosity model. Therefore, other factors act on the variation of the flow shear rate and resulting shear stress. In particular, the flow rate ratio, as defined in (29), which has a direct influence on the shear rate in the flow, which
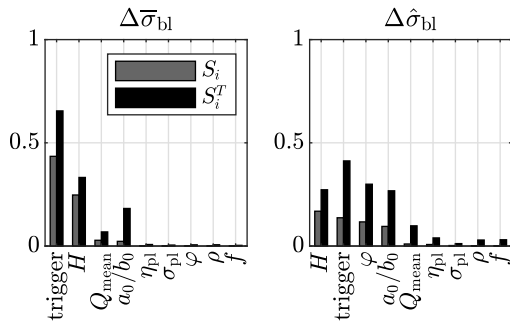
Fig. 11. Sensitivity indices of the global analysis between different model assumption on the mean value of blood conductivity change (left) and on its amplitude (right). The variables are sorted by first-order sensitivity index.

further influences the RBCs deformed configuration in (2). Besides, the undeformed configuration of the RBCs a_0/b_0 is as crucial as φ in the final computation of the amplitude of blood conductivity change $\Delta\hat{\sigma}_{bl}$. Finally, once the deformation of the RBCs has taken place, the C factor of (4) is consequently affected.

The sensitivity analysis among the model assumptions is presented in Fig. 11. Again, the left part of the figure represents the first- and total-order sensitivity indices of the cycle average of the blood conductivity change $\Delta\overline{\sigma}_{bl}$. In contrast, the right picture refers to the QoI amplitude of blood conductivity change $\Delta\hat{\sigma}_{bl}$. As expected, the change of the model assumptions affects both outputs largely, since the *trigger* factor has the highest first-order sensitivity index. These results stress the need for a clear identification of the model that is used for the computation of both QoIs. However, although the *trigger*'s first-order sensitivity index S_i is dominant on the other indices for the computation of $\Delta\overline{\sigma}_{bl}$, the first Sobol' index of the same input random variable has a much lower value for the amplitude of $\Delta\sigma_{bl}$. Furthermore, its value shares a similar value to the indices of the blood haematocrit level H.

When computing the amplitude of blood conductivity change, the model shows a high interaction between the input random variables, as it is visible by the higher values of S_i^T in Fig. 11 right with respect to the S_i. This translates in non-additive model behaviour, besides being non-linear. However, such high interaction effect seems to disappear when it is about the QoI $\Delta\overline{\sigma}_{bl}$.

5. Conclusions

The study showed how to reduce the uncertainty of electrical conductivity of flowing blood and analysed the impact of different model assumptions on such blood property. The conductivity model described in Section 2.1 is coupled with three different fluid mechanics model assumptions, namely Newtonian fluid and steady flow, Newtonian fluid and harmonically pulsating flow, non-Newtonian fluid and harmonically pulsating flow. A global sensitivity analysis (gSA) is performed within fluid mechanics models, and among them in order to better understand the impact of such assumptions. Given the scope of the study that is to reduce the variability in the model outputs, a variance-based method and a surrogate model, i.e. polynomial chaos expansion, are employed. The surrogate model is solved either with ordinary least square (OLS) or with the least-angle regression (LARS), which selection is due to the computational cost of each model assumption. The computation of the Sobol indices as quantitative measures of input factors sensitivity is performed through the solution of the surrogate model. Other sensitivity analysis methods, e.g. non-parametric or density-based, are discarded from this study due to the unclear behaviour of the model prior to the analysis.

Two outputs are considered as quantities of interest: the average value over one cardiac cycle of the blood conductivity change $\Delta\sigma_{bl}$ and its amplitude, namely $\Delta\overline{\sigma}_{bl}$ and $\Delta\hat{\sigma}_{bl}$.

Initial analysis of the distribution of the results underlines the inability of a steady flow model assumption in representing the natural behaviour of the blood conductivity changes and, as might be expected, its amplitude response. Therefore, a steady flow model assumption is left out from the sensitivity analysis and considered inadequate for the aim of the study.

The sensitivity analysis shows that the haematocrit level of the blood generally has the highest effect on the average value of the conductivity change of blood for both a Newtonian and non-Newtonian formulation of the fluid. Such a result is confirmed by the theoretical formulation of the problem that has been primarily investigated in the past literature. These research works stress indeed the effect that non-conductive red blood cells have on the computation of blood conductivity. However, switching to a shear-thinning generalized model for the computation of the conductivity change amplitude, the effect of the haematocrit level of the blood loses its dominance in the influence of the model in favour of the flow rate ratio between pulsating and steady flow and the undeformed RBCs axes ratio. This change in model mechanics better represents the physicality of the electrical characteristics of blood. Therefore, the non-Newtonian formulation enables a different path for the computation of the changes in the conductivity of blood, considering the pulsation of the flow and the patient-specific characteristics of the RBCs. This random variable was demonstrated to be more influential than the haematocrit level. In conclusion, given the different results from the sensitivity analysis for the two model responses, the choice of the quantity of interest for any further computation has to be thoughtfully considered. Further development of the flow model, including physiologically accurate volumetric flow rates and elasticity of the pipe wall, may deepen these investigations and initiate to new scientific challenges.

CRediT authorship contribution statement

Gian Marco Melito: Conceptualization, Writing - original draft, Visualization, Methodology, Software, Writing - review & editing, Formal analysis. **Thomas Stephan Müller:** Conceptualization, Writing - original draft, Visualization, Methodology, Software, Writing - review & editing. **Vahid Badeli:** Conceptualization, Writing - original draft, Visualization, Writing - review & editing. **Katrin Ellermann:** Writing - review & editing, Supervision. **Günter Brenn:** Writing - review & editing, Supervision. **Alice Reinbacher-Köstinger:** Writing - review & editing, Supervision.

Declaration of competing interest

The authors declare that they have no known competing financial interests or personal relationships that could have appeared to influence the work reported in this paper.

Acknowledgements

References

[1] Merrill E. Rheology of blood. Physiol Rev 1969;49(4):863–88. http://dx.doi.org/10.1152/physrev.1969.49.4.863.

[2] Merrill E, Gilliland ER, Cokelet G, Shin H, Britten A, Wells RE. Rheology of human blood, near and at zero flow: effects of temperature and hematocrit level. Biophys J 1963;3(3):199–213. http://dx.doi.org/10.1016/S0006-3495(63)86816-2.

[3] Frewer RA. The electrical conductivity of flowing blood. Biomed Eng 1974;9(12):552–5.

[4] Visser KR. Electric properties of flowing blood and impedance cardiography. Ann Biomed Eng 1989;17(5):463–73. http://dx.doi.org/10.1007/BF02368066.

[5] Fåhræus R, Lindqvist T. The viscosity of the blod in narrow capillary tubes. Am Physiol Soc 1931;96(3):562–8. http://dx.doi.org/10.1152/ajplegacy.1931.96.3.562.

[6] Wells R, Merrill EW. The variability of blood viscosity. Am J Phys Med 1961;31(4):505–9. http://dx.doi.org/10.1016/0002-9343(61)90134-6.

[7] Thurston G. Viscoelasticity of human blood. Biophys J 1972;12:1205–17. http://dx.doi.org/10.1016/S0006-3495(72)86156-3.

[8] Chien S, Usami S, Dellenback RJ, Gregersen MI. Shear-dependent deformation of erythrocytes in rheology of human blood. Am Physiol Soc 1970;219(1):136–42. http://dx.doi.org/10.1152/ajplegacy.1970.219.1.136.

[9] Bera TK. Bioelectrical impedance methods for noninvasive health monitoring: a review. J Med Biol Eng 2014;2014. http://dx.doi.org/10.1155/2014/381251.

[10] Ulbrich M, Mühlsteff J, Leonhardt S, Walter M. Influence of physiological sources on the impedance cardiogram analyzed using 4D FEM simulations. Physiol Meas 2014;35(7):1451. http://dx.doi.org/10.1088/0967-3334/35/7/1451.

[11] Reinbacher-Köstinger A, Badeli V, Biro O, Magele C. Numerical simulation of conductivity changes in the human thorax caused by aortic dissection. IEEE Trans Magn 2019;55(6):1–4. http://dx.doi.org/10.1109/TMAG.2019.2895418.

[12] Fricke H. A mathematical treatment of the electric conductivity and capacity of disperse systems I. The electric conductivity of a suspension of homogeneous spheroids. Phys Rev 1924;24:575–87. http://dx.doi.org/10.1103/PhysRev.24.575.

[13] Maxwell JC. A treatise on electricity and magnetism, vol. 1. Clarendon press; 1881.

[14] Edgerton RH. Conductivity of sheared suspensions of ellipsoidal particles with application to blood flow. IEEE Trans Biomed Eng 1974;(1):33–43. http://dx.doi.org/10.1109/TBME.1974.324359.

[15] Visser KR. Electric conductivity of stationary and flowing human blood at low frequencies. In: Images of the twenty-first century. proceedings of the annual international engineering in medicine and biology society. IEEE; 1989, p. 1540–2. http://dx.doi.org/10.1109/IEMBS.1989.96329.

[16] Sakamoto K, Kanai H. Electrical characteristics of flowing blood. IEEE Trans Biomed Eng 1979;(12):686–95. http://dx.doi.org/10.1109/TBME.1979.326459.

[17] Fujii M, Nakajima K, Sakamoto K, Kanai H. Orientation and deformation of erythrocytes in flowing blood. Ann New York Acad Sci 1999;873(1):245–61. http://dx.doi.org/10.1111/j.1749-6632.1999.tb09473.x.

[18] Hoetink A, Faes TJ, Visser K, Heethaar RM. On the flow dependency of the electrical conductivity of blood. IEEE Trans Biomed Eng 2004;51(7):1251–61. http://dx.doi.org/10.1109/TBME.2004.827263.

[19] Gaw RL, Cornish BH, Thomas BJ. The electrical impedance of pulsatile blood flowing through rigid tubes: an experimental investigation. In: 13th international conference on electrical bioimpedance and the 8th conference on electrical impedance tomography. Springer; 2007, p. 73–6.

[20] Gaw RL, Cornish BH, Thomas BJ. Comparison of a theoretical impedance model with experimental measurements of pulsatile blood flow. In: 13th international conference on electrical bioimpedance and the 8th conference on electrical impedance tomography. Springer; 2007, p. 32–5.

[21] Gaw RL, Cornish BH, Thomas BJ. The electrical impedance of pulsatile blood flowing through rigid tubes: a theoretical investigation. IEEE Trans Biomed Eng 2008;55(2):721–7. http://dx.doi.org/10.1109/TBME.2007.903531.

[22] Womersley J. Oscillatory flow in arteries: the constrained elastic tube as a model of arterial flow and pulse transmission. Phys Med Biol 1957;2(2):178–87.

[23] Shen H, Li S, Wang Y, Qin K-R. Effects of the arterial radius and the center-line velocity on the conductivity and electrical impedance of pulsatile flow in the human common carotid artery. Med Biol Eng Comput 2019;57(2):441–51. http://dx.doi.org/10.1007/s11517-018-1889-x.

[24] Walker H, Hall WD, Hurst JW. Clinical methods: The history, physical, and laboratory examinations. third ed.. Boston : Butterworths; 1990.

[25] Mutua D, Njagi ENM, Orinda GO. Hematological profile of normal pregnant women. J Blood Lymph 2018;8(2):1–6. http://dx.doi.org/10.4172/2165-7831.1000220.

[26] Vergouwen P, Collee T, Marx J. Haematocrit in elite athletes. Int J Sports Med 1999;20(08):538–41.

[27] Saltelli A, Annoni P, Azzini I, Campolongo F, Ratto M, Tarantola S. Variance based sensitivity analysis of model output. Design and estimator for the total sensitivity index. Comput Phys Commun 2010;181(2):259–70.

[28] Eck VG, Donders WP, Sturdy J, Feinberg J, Delhaas T, Hellevik LR, Huberts W. A guide to uncertainty quantification and sensitivity analysis for cardiovascular applications. Int J Numer Methods Biomed Eng 2016;32(8).

[29] Sudret B. Global sensitivity analysis using polynomial chaos expansions. Reliab Eng Syst Saf 2008;93(7):964–79.

[30] Le Gratiet L, Marelli S, Sudret B. Metamodel-based sensitivity analysis: Polynomial chaos expansions and Gaussian processes. In: Ghanem R, Higdon D, Owhadi H, editors. Handbook of uncertainty quantification. Cham: Springer International Publishing; 2017, p. 1289–325. http://dx.doi.org/10.1007/978-3-319-12385-1_38.

[31] Kass RE, Raftery AE. Bayes Factors. J Am Stat Assoc 1995;90(430):773–95.

[32] Hoeting JA, Madigan D, Raftery AE, Volinsky CT. Bayesian model averaging: a tutorial. Stat Sci 1999;382–401.

[33] Jia W, McPherson B, Pan F, Dai Z, Xiao T. Uncertainty quantification of CO2 storage using Bayesian model averaging and polynomial chaos expansion. Int J Greenh Gas Control 2018;71:104–15.

[34] Saltelli A, Tarantola S, Campolongo F, Ratto M. Sensitivity analysis in practice: a guide to assessing scientific models, vol. 1. Wiley Online Library; 2004.

[35] Saltelli A, Ratto M, Andres T, Campolongo F, Cariboni J, Gatelli D, Saisana M, Tarantola S. Global sensitivity analysis: the primer. John Wiley & Sons; 2008.

[36] Saisana M, Saltelli A, Tarantola S. Uncertainty and sensitivity analysis techniques as tools for the quality assessment of composite indicators. J Roy Statist Soc Ser A 2005;168(2):307–23.

[37] Tarantola S, Corradi A, Ruffo P, Saltelli A. Global sensitivity analysis techniques for the analysis of the oil potential of sedimentary beams. 2001.

[38] Saltelli A, Ratto M, Tarantola S, Campolongo F, Commission E, et al. Sensitivity analysis practices: Strategies for model-based inference. Reliab Eng Syst Saf 2006;91(10–11):1109–25.

[39] Saltelli A. Making best use of model evaluations to compute sensitivity indices. Comput Phys Commun 2002;145(2):280–97.

[40] Bitbol M, Quemada D. Measurement of erythrocyte orientation in flow by spin labeling. Biorheology 1985;22(1):31–42. http://dx.doi.org/10.3233/BIR-1985-22103.

[41] Bitbol M, Leterrier F. Measurement of the erythrocyte orientation in a flow by spin labeling. Biorheology 1982;19(6):669–80. http://dx.doi.org/10.3233/BIR-1982-19601.

[42] Bird R, Armstrong RC, Hassager O. Dynamics of polymeric liquids - volume 1 fluid mechanics. A Wiley-Interscience puplication; 1987.

[43] Böhme G. Strömungsmechanik nicht-newtonscher Fluide (Mechanics of non-Newtonian Fluids, in German). B.G. Teubner-Verlag; 2000.

[44] Carreau P. Rheological equations from molecular network theories [Ph.D. thesis], University of Wisconsin, Madison; 1968, http://dx.doi.org/10.1122/1.549276.

[45] Metzner A, Reed JC. Flow of non-newtonian fluids - correlation of the laminar, transition, and turbulent-flow regions. Am Inst Chem Eng 1955;1(4):434–40. http://dx.doi.org/10.1002/aic.690010409.

[46] Womersley J. Method for the calculation of velocity, rate of flow and viscous drag in arteries when the pressure gradient is known. J Physiol 1955;127:553–63. http://dx.doi.org/10.1113/jphysiol.1955.sp005276.

[47] Borgonovo E, Plischke E. Sensitivity analysis: a review of recent advances. European J Oper Res 2016;248(3):869–87.

[48] Iooss B, Lemaître P. A review on global sensitivity analysis methods. In: Uncertainty management in simulation-optimization of complex systems. Springer; 2015, p. 101–22.

[49] Iooss B, Saltelli A. Introduction to sensitivity analysis. 2015, p. 1–20. http://dx.doi.org/10.1007/978-3-319-11259-6_31-1.

[50] Saltelli A, Tarantola S, Campolongo F, et al. Sensitivity anaysis as an ingredient of modeling. Statist Sci 2000;15(4):377–95.

[51] Borgonovo E, Apostolakis GE. A new importance measure for risk-informed decision making. Reliab Eng Syst Saf 2001;72(2):193–212.

[52] Borgonovo E, Peccati L. Sensitivity analysis in investment project evaluation. Int J Prod Econ 2004;90(1):17–25.

[53] Morris MD. Factorial sampling plans for preliminary computational experiments. Technometrics 1991;33(2):161–74.

[54] Efron B, Stein C. The jackknife estimate of variance. Ann Statist 1981;586–96.

[55] Rabitz H, Aliş ÖF. General foundations of high-dimensional model representations. J Math Chem 1999;25(2–3):197–233.

[56] Oakley JE, O'Hagan A. Probabilistic sensitivity analysis of complex models: a Bayesian approach. J R Stat Soc Ser B Stat Methodol 2004;66(3):751–69.

[57] Sobol IM. Sensitivity estimates for nonlinear mathematical models. Math Model Comput Exp 1993;1(4):407–14.

[58] Borgonovo E. A new uncertainty importance measure. Reliab Eng Syst Saf 2007;92(6):771–84.

[59] Pianosi F, Wagener T. A simple and efficient method for global sensitivity analysis based on cumulative distribution functions. Environ Model Softw 2015;67:1–11.

[60] Iman RL, Conover WJ. The use of the rank transform in regression. Technometrics 1979;21(4):499–509.

[61] Saltelli A, Sobol IM. About the use of rank transformation in sensitivity analysis of model output. Reliab Eng Syst Saf 1995;50(3):225–39.

[62] Sobol IM. On sensitivity estimation for nonlinear mathematical models. Matematicheskoe Modelirovanie 1990;2(1):112–8.

[63] Sobol IM. Global sensitivity indices for nonlinear mathematical models and their Monte Carlo estimates. Math Comput Simul 2001;55(1–3):271–80.

[64] Mohiaddin RH, Kilner PJ, Rees S, Longmore DB. Magnetic resonance volume flow and jet velocity mapping in aortic coarctation. J Am Coll Cardiol 1993;22(5):1515–21.

[65] Hinghofer-Szalkay H. Method of high-precision microsample blood and plasma mass densitometry. J Appl Physiol 1986;60(3):1082–8.

[66] Hinghofer-Szalkay H, Greenleaf J. Continuous monitoring of blood volume changes in humans. J Appl Physiol 1987;63(3):1003–7.

[67] Kenner T. The measurement of blood density and its meaning. Basic Res Cardiol 1989;84(2):111–24.

[68] Gaw RL. The effect of red blood cell orientation on the electrical impedance of pulsatile blood with implications for impedance cardiography [Ph.D. thesis], Queensland University of Technology; 2010.

[69] Martini F, Timmons MJ. Fundamentals of human anatomy and physiology. Prentice Hall; 1995.

[70] Thibodeau GA, Patton KT. Anatomy and physiology 4° edition. Support Movement 1999;162–314.

[71] Ghanem RG, Spanos PD. Stochastic finite elements: a spectral approach. Courier Corporation; 2003.

[72] Xiu D, Karniadakis GE. Modeling uncertainty in steady state diffusion problems via generalized polynomial chaos. Comput Methods Appl Mech Engrg 2002;191(43):4927–48.

[73] Wiener N. The homogeneous chaos. Amer J Math 1938;60(4):897–936.

[74] Crestaux T, Le Maıtre O, Martinez J-M. Polynomial chaos expansion for sensitivity analysis. Reliab Eng Syst Saf 2009;94(7):1161–72.

[75] Marelli S, Sudret B. UQLab: A framework for uncertainty quantification in Matlab. In: Vulnerability, uncertainty, and risk: quantification, mitigation, and management. 2014, p. 2554–63.

[76] Stalder A, Frydrychowicz A, Russe MF, Korvink JG, Henning J, Li K, Markl M. Assessment of flow instabilities in the healthy aorta using flow-sensitive MRI. J Magn Reson Imaging 2011;33:839–46. http://dx.doi.org/10.1002/jmri.22512.

[77] Berveiller M, Sudret B, Lemaire M. Presentation of two methods for computing the response coefficients in stochastic finite element analysis. In: Proc. 9th ASCE specialty conference on probabilistic mechanics and structural reliability. Albuquerque, USA; 2004.

[78] Berveiller M, Sudret B, Lemaire M. Stochastic finite element: a non intrusive approach by regression. Eur J Comput Mech 2006;15(1–3):81–92.

[79] Blatman G, Sudret B. Adaptive sparse polynomial chaos expansion based on least angle regression. J Comput Phys 2011;230(6):2345–67.

[80] Blatman G, Sudret B. An adaptive algorithm to build up sparse polynomial chaos expansions for stochastic finite element analysis. Probab Eng Mech 2010;25(2):183–97.

[81] Marelli S, Lüthen N, Sudret B. UQLab user manual – Polynomial chaos expansions. Technical Report, Chair of Risk, Safety and Uncertainty Quantification, ETH Zurich, Switzerland; 2021, Report # UQLab-V1.4-104.